ChemComm

COMMUNICATION

View Article Online
View Journal | View Issue

Cite this: *Chem. Commun.*, 2025, **61**, 8727

Received 27th February 2025,
Accepted 7th April 2025

DOI: 10.1039/d5cc01090j

rsc.li/chemcomm

Systematic exploration of alkali–anion pairs for descriptor identification in OH-mediated methane coupling†

Shintaro Yoshida, William J. Movick, Keisuke Obata and Kazuhiro Takanabe *

The oxidative coupling of methane (OCM) was investigated using various alkali metal salts supported on SiO_2. The addition of H_2O enhances both the methane conversion rate and selectivity across all alkali metal salts, which suggests there is an OH-radical-mediated pathway that is facilitated by the surface formation of alkali peroxide. To explain the observed experimental differences, we explored the interactive energetics of alkali–anion pairs with a particular focus on the stabilization of alkali peroxide intermediates by anion species. Anion polarizability is indicative of the alkali ion's degree of freedom and positively correlated with the catalytic performance due to formation capability of catalytic alkali peroxide species. This insight highlights the critical role of the reaction of surface alkali peroxide with H_2O as a key elementary step in OCM.

The oxidative coupling of methane (OCM) involves the reaction of CH_4 directly with O_2 at high temperatures ($>\sim$600 °C) to produce C_2 products (C_2H_6, C_2H_4) over heterogeneous catalysts.[1] The design of relevant catalysts is centered around improving selectivity to C_2 products over CO_x (CO_2, CO). C_2 formation occurs *via* the gas-phase coupling of CH_3 radicals[2] with CH_3 generated on the catalyst surface. Thus, the integration of surface and gas-phase reactions is required to describe the reaction adequately.[3–5]

Supported alkali metal tungstate catalysts stand out for having the highest selectivity towards C_2 products since the first reports of Mn–Na_2WO_4/SiO_2.[6] Various reports have argued that WO_4^{2-} acts as the CH_3 formation site. However, the reported mechanisms vary and have included the involvement of WO_4^{2-} lattice oxygen,[7,8] surface-derived O_2^-,[9,10] and surface $NaWO_x$ species.[11,12] The roles of both Na[13] and Mn[14] have been reported to involve the distortion of the WO_4^{2-} centers. In addition, H_2O is known to have a promotional effect by accelerating CH_4 conversion and improving C_2 selectivity,[15] which complicates the kinetic analysis. Zanina *et al.* suggested that H_2O has a role in the removal of CO_x-selective peroxide-type O_2 surface species.[8,16] However, Wang *et al.*[17] reported that surface O_2 species selectively form C_2 products, while Liu *et al.*[18] attributed the H_2O effect to the formation of Si–OH surface species.

Our research group has argued that the selective formation of CH_3 radicals involves OH-radical intermediates that are generated by H_2O and O_2 reacting on the Na sites of the catalyst surface (possibly from H_2O_2 release).[19] This mechanism can be described by the following:

$$O_2 + A_2\text{–}MO_x \rightarrow A_2O_2\text{–}MO_x \quad (1)$$

$$A_2O_2\text{–}MO_x + H_2O \rightarrow H_2O_2 + A_2\text{–}MO_x \quad (2)$$

$$H_2O_2 \rightarrow 2OH^{\bullet} \quad (3)$$

$$OH^{\bullet} + CH_4 \rightarrow CH_3^{\bullet} + H_2O \quad (4)$$

$$2CH_3^{\bullet} \rightarrow C_2H_6 \quad (5)$$

where A is the alkali cation, and A_xMO_4 represents the bulk catalyst. Gas phase reactions (3)–(5) have been demonstrated to be C_2 selective,[20] although H_2O_2 has not been observed directly.

Alkali metal peroxide intermediates have been observed by near-atmospheric-pressure X-ray photoelectron spectroscopy (XPS) on K_2WO_4[21] and Na_2WO_4[22] catalysts, and OH radical generation has been observed using laser fluorescence. Alkali metal peroxides are expected to be the key surface intermediate and likely generate either OH radicals directly or H_2O_2,[23] which subsequently decomposes into two OH radicals (eqn (2)). Thus, the catalyst's effectiveness will depend on the presence of an alkali metal salt, regardless of the identity of the cation or anion.

Systematic modification of alkali metal cations is common in the catalytic literature.[24,25] Zanina *et al.* investigated the effect of the identity of the alkali metal cation,[26,27] and Palermo *et al.*[28] confirmed that various alkali metals can be effective for OCM. In addition, studies have been conducted on the effects of changing the anion. Supported alkali metal MoO_4^{2-} has been shown to be effective for OCM (LiCl–Na_2MoO_4),[29] partial CH_4 oxidation ((Li, Na, K, Rb, Cs)$_2MoO_4/SiO_2$),[30] and nonoxidative

Department of Chemical System Engineering, School of Engineering, The University of Tokyo, 7-3-1 Hongo, Bunkyo-ku, Tokyo, Japan.
E-mail: takanabe@chemsys.t.u-tokyo.ac.jp

† Electronic supplementary information (ESI) available: Experimental methods, activity and selectivity breakdown, catalyst characterization, and additional correlation plots. See DOI: https://doi.org/10.1039/d5cc01090j

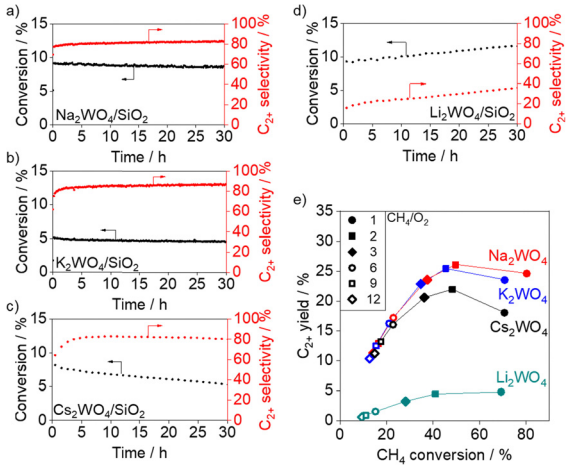

Fig. 1 CH_4 conversion and C_{2+} selectivity as a function of time on stream for (a) Na_2WO_4/SiO_2, (b) K_2WO_4/SiO_2, (c) Cs_2WO_4/SiO_2, and (d) Li_2WO_4/SiO_2 at 850 °C with 10 kPa CH_4 and 1.7 kPa O_2 (balance Ar) using 0.1 g catalyst and 30 mL min^{-1} flow. (e) Maximum achievable C_{2+} yield as a function of CH_4 conversion at varying CH_4/O_2 ratios (maintaining 10 kPa CH_4 and adjusting O_2 pressure). Detailed results are summarized in Table S1 (ESI†).

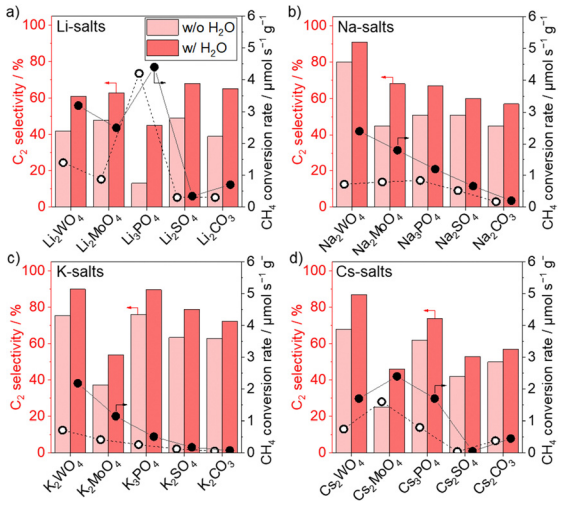

Fig. 2 CH_4 conversion rate and C_2 selectivity of (a) Li-salt catalysts, (b) Na-salt catalysts, (c) K-salt catalysts, and (d) Cs-salt catalysts on SiO_2 for OCM at 850 °C with 10 kPa CH_4 and 1.7 kPa O_2 (balance Ar) using 0.2 g catalyst and 30–150 mL min^{-1} flow extrapolated to 1% CH_4 conversion. Detailed results are listed in Table S2 (ESI†).

CH_4 aromatization (K_2MoO_4/ZSM-5).[31] Both Na_2SO_4/SiO_2[32] and K_2MnO_4/SiO_2[33] have also been shown to be effective for OCM, with the latter showing a promotional effect of H_2O. A systematic modification of the metal anion was conducted by Hou *et al.* on Mn-promoted Na-salts which focused on the anion–Mn interaction.[34] Both variables need to be examined to accurately determine the kinetic impact of varying cation and anion species in the alkali metal salt catalysts.

The aim of the present study was to fill the gaps in the research by examining a wide variety of alkali metal salt catalysts for OCM with a focus on the promotional effect of H_2O. The OCM reaction rate and selectivity were measured using a fixed-bed plug flow reactor (PFR) with a U-shaped tube. Fig. 1 shows the CH_4 conversion rate and C_{2+} selectivity (including hydrocarbons larger than C_2) as a function of time on stream for M_2WO_4/SiO_2 catalysts (where M represents Li, Na, K, or Cs) at 850 °C and a CH_4/O_2 ratio of 6. For the cations Na, K, and Cs, the CH_4 conversion decreased over time, while C_{2+} selectivity increased. The decrease in CH_4 conversion rate can result from either sintering of the catalyst or the desorption of the active M_2WO_4, which reduces the number of active sites. Cs_2WO_4/SiO_2 showed lower durability than the other catalysts, likely due to the low melting point (350 °C) of Cs_2WO_4 compared to Na_2WO_4 (698 °C) and K_2WO_4 (921 °C). In contrast, Li_2WO_4/SiO_2 showed increases in both the CH_4 conversion and C_2 selectivity over time, but the C_2 selectivity was much lower.

The maximum achievable C_{2+} yield was achieved at a CH_4/O_2 ratio of 2 for most samples, as is shown in Fig. 1e. Both Na_2WO_4/SiO_2 and K_2WO_4/SiO_2 showed similar obtainable C_{2+} yield, with Na_2WO_4 reaching 26.1%. Cs_2WO_4/SiO_2 showed similar results but had a lower yield due to the lower selectivity towards C_{2+} products, particularly at lower CH_4/O_2 ratios. This indicates a higher tendency towards product oxidation. Li_2WO_4/SiO_2 showed significantly lower C_{2+} yield and only reached 4.8% at a CH_4/O_2 ratio of 1. This was clearly due to the low selectivity of this catalyst compared to the other alkali metal tungstate catalysts.

Next, various cations (Li, Na, K, and Cs) were introduced with various anions (WO_4^{2-}, MoO_4^{2-}, SO_4^{2-}, PO_4^{3-}, and CO_3^{2-}) and tested for their OCM performance. Alkali metal salts (5 wt%) on SiO_2 were prepared using the wet impregnation method. Fig. 2 shows the C_2 selectivity and CH_4 conversion rate for each catalyst. Alkali metal salts were expected to remain on the surface of the SiO_2 based on observation of XPS (Fig. S1–S16, ESI†). The results were measured at 850 °C with 1% CH_4 conversion, 10 kPa of CH_4, and 1.7 kPa of O_2 ($CH_4/O_2 = 6$) with either 1.7 kPa H_2O (wet) added at the inlet or without H_2O addition (dry). The WO_4^{2-} anion, particularly with Na_2WO_4/SiO_2 and K_2WO_4/SiO_2, showed the best C_2 selectivity with high CH_4 conversion rates. The MoO_4^{2-} anions also showed high CH_4 conversion rates but were limited by low C_2 selectivity. The SO_4^{2-}, PO_4^{3-}, and CO_3^{2-} anions typically showed significantly lower CH_4 conversion rates.

The alkali metal also showed an impact on the OCM performance. Na^+ and K^+ typically had higher C_2 selectivity, and Li^+ showed lower C_2 selectivity. However, all catalysts showed a clear promotional effect of H_2O for C_2 selectivity and CH_4 conversion. Although the promotional effect is unique to alkali metal salts, all instances of them universally show H_2O promotion, which is a strong indicator that these catalysts share a similar reaction mechanism.

The catalysts showed a wide range of physical properties after the initial synthesis and calcination at 900 °C. The measured surface areas (Table S3, ESI†) were 0.7–32 m^2 g^{-1}. Much of the loss of surface area was due to transformation of amorphous SiO_2 into the cristobalite phase, which was catalyzed by the alkali metals (Table S4, ESI†). However, some catalysts were not able to fully transform the SiO_2, and it remained amorphous (Table S4 and Fig. S17, ESI†). This is known to decrease C_2

selectivity. In addition, the catalyst loading measured by atomic adsorption spectroscopy (AAS) and inductively coupled plasma (ICP) had a wide range. Samples with the CO_3^{2-} anion showed the largest loss of catalyst content due to thermal decomposition (Table S4, ESI†).

In contrast, the ratio of CH_4 conversion under wet conditions to that under dry conditions (r_{wet}/r_{dry}) should be relatively unaffected by textural and metal loading differences. The value of r_{wet}/r_{dry} should directly correlate to the catalyst's capacity towards the OH-radical-mediated pathway, in addition to the overall effectiveness of the catalyst. The r_{wet}/r_{dry} is also insensitive to the loss of catalyst species during the high temperature reaction. Cs_2WO_4/SiO_2 showed a similar C_2 selectivity to Na_2WO_4/SiO_2 at low conversion, whereas at high conversion (Fig. 1e), Cs_2WO_4/SiO_2 showed much lower performance, which can be correlated to a lower r_{wet}/r_{dry} for this catalyst. When considering the OH-radical-mediated pathway, the first step in the reaction was postulated to be the formation of an alkali peroxide from the surface alkali metal oxide according to eqn (1). Therefore, alkali metal peroxide formation is critical to the OCM performance.

The order of the r_{wet}/r_{dry} results (and thus the OH radical formation ability) can be related to several physical properties of the anion species. Fig. 3 shows r_{wet}/r_{dry} as a function of the formation energy for each alkali metal. The r_{wet}/r_{dry} ratio generally increased with increasing formation energy. In addition, the relative effectiveness of the anion can be clearly seen, and the highest H_2O promotion was observed in the order of $WO_4^{2-} > MoO_4^{2-} > PO_4^{3-} > SO_4^{2-}$.

A selection of physical properties of anions is shown in Table 1. The polarizability of WO_4^{2-} and MoO_4^{2-} were not directly tabulated in the literature, but estimates were obtained from reported dielectric factors (see ESI† for details, Table S5). The anionic radii and polarizability increased in order of $WO_4^{2-} > MoO_4^{2-} > PO_4^{3-} > SO_4^{2-}$, which tracks with the order of r_{wet}/r_{dry}. Both the anionic radius and polarizability correlate to the relative flexibility of the anion. Larger anions will have a lower average charge density and thus have higher polarizability. The increase in polarizability allows for dispersion of the negative charge on the anion. The distributed charge allows for the anions to be distorted more easily. In addition, the reported pK_a values of the corresponding protonic acids (H_xMO_4; Table 1) increase with r_{wet}/r_{dry}. The pK_a values correlate with the decreases in relative acidity with increasing ion radius, although it was measured in very different conditions (aqueous phase, room temperature) than those used for OCM. However, there is still a clear relationship between these parameters and the OH radical formation ability of the catalysts.

Table 1 Chemical properties of anion species

Anion[a]	Ionic radius/pm[a]	Polarizability/Å^{-3}	pK_a[d]
WO_4^{2-}	237	9.9–10.0[b]	3.6–5.1[e]
MoO_4^{2-}	231	6.7–8.1[b]	4–4.2[f]
PO_4^{3-}	230	6.8[c]	2.2
SO_4^{2-}	218	5.1[c]	−3

[a] Values obtained from Simoes *et al.*[33] [b] Estimated from dielectric factor, see ESI for details. [c] Obtained from Hou *et al.*[34] [d] Reported pK_a values of H_xMO_4. [e] Values obtained from Li *et al.*[35] [f] Values obtained from Goldberg.[36]

The properties of the anions listed in Table 1 are related to the relative structural degree of freedom according to the anion species. The alkali (su)peroxide species are highly unstable and even volatile under OCM condition. Stronger bonds between cation–anion species allow the alkali metal to stay on the surface of the catalyst, which limits the range of available positions to form peroxide surface intermediate species. A flexible anion allows for higher alkali metal mobility, which is likely to allow for O_2 chemisorption and the formation of alkali metal peroxide bonds. Intuitively, heavier anions (WO_4^{2-}, MoO_4^{2-}) have higher polarizability than the lighter anions (PO_4^{3-}, SO_4^{2-}), which helps to explain why these anions are typically the only ones viable for OCM. WO_4^{2-} shows much larger polarizability than the other anions, in addition to a distinctively large value of r_{wet}/r_{dry}.

The cations are the active sites in the OH radical mechanism, and their effect was also investigated. The critical step of the reaction is the formation of the alkali metal peroxide (A_2O_2), so the values of r_{wet}/r_{dry} were correlated to the A_2O_2 formation energy from the alkali metal oxide (A_2O, Fig. S18, ESI†). The highest r_{wet}/r_{dry} value of WO_4-related catalysts occurred with Na and K, reaching 2.5 and 2.7, respectively. Both Na_2O_2 (−98 kJ mol^{-1}) and K_2O_2 (−133 kJ mol^{-1}) have moderate formation energies compared to Li_2O_2 (−34 kJ mol^{-1}) and Cs_2O_2 (−311 kJ mol^{-1}). If the formation energy is too low, it will limit the stability of A_2O_2 and decrease the overall rate. If it is too high, it will over-stabilize the A_2O_2 and limit further reaction to form either H_2O_2 or OH radicals. However, this correlation is only observed with WO_4 and loosely with SO_4. MoO_4 showed the highest r_{wet}/r_{dry} on Li_2MoO_4/SiO_2, while PO_4 showed the highest with Cs_3PO_4/SiO_2. In addition, the cation effect was much weaker in comparison to the observed anion effect. The nature of the anion is clearly more important for the OCM performance than the nature and identity of the alkali metal cations.

Direct observation of the alkali metal salt bonding was attempted, but it was difficult due to the gap between OCM

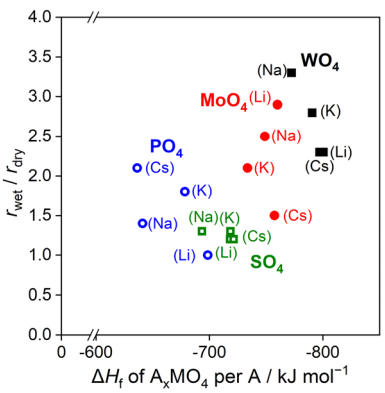

Fig. 3 Ratio of wet (1.7 kPa H_2O added) over dry (no additional H_2O) CH_4 conversion rate as a function of formation enthalpy of the catalyst salt. Rates were determined at 1% CH_4 conversion and 850 °C with 10 kPa CH_4, 1.7 kPa O_2, and balance Ar.

conditions and available characterization techniques. XPS (Fig. S19, ESI†) was used to observe binding-energy differences on either the alkali metal (Li, Na, K, or Cs) or anion species (W, Mo, P, or S). In the case of both Na and W, decreasing binding energy led to an increased r_{wet}/r_{dry}. The lower binding energy can be an indicator of lower bond strength, which is likely correlated to higher polarizability. However, this trend was not as clear with the other samples, likely due to the measurement being conducted ex situ. *In situ* Raman spectroscopy was also used to observe the W–O and Mo–O bonding at 800 °C (Fig. S20, ESI†), and similar spectra were observed between Na_2WO_4 and K_2WO_4, as well as Li_2MoO_4 and K_2MoO_4. Additional antistretching W–O modes were observed for Li_2WO_4 and Cs_2WO_4. This was also observed for Na_2MoO_4 and Cs_2MoO_4 and may be related to the low selectivity of these samples. However, structural changes that occur at 800 °C can be complicated and further work would be needed to fully understand these changes.

In conclusion, we have confirmed that alkali metal salts universally play a major role in the selective promotion of OCM through the addition of water for the OH radical mechanism. Although the alkali metal is an active site for OH radical formation through their peroxide form, the counter anion has a major influence on its activity and stability to form these unstable alkali peroxide intermediate, resulting in a stronger promotional effect of H_2O. Although different cations certainly influenced this effect, anions were found to play a more significant role in the formation of optimized surface active sites for OH radical formation. This work gives insight into why WO_4-based catalysts consistently show the highest performance for OCM reactions.

This work was supported in part by MHI Innovation Accelerator LLC. K. O. acknowledges JSPS KAKENHI (Grant Number 23K13594).

Data availability

The data supporting this article have been included as part of the ESI.†

Conflicts of interest

There are no conflicts to declare.

References

1 G. E. Keller and M. M. Bhasin, *J. Catal.*, 1982, **73**, 9–19.
2 K. D. Campbell and J. H. Lunsford, *J. Phys. Chem.*, 1988, **92**, 5792–5796.
3 J. Sadeghzadeh Ahari, S. Zarrinpashne and M. T. Sadeghi, *Fuel Process. Technol.*, 2013, **115**, 79–87.
4 T. P. Tiemersma, M. J. Tuinier, F. Gallucci, J. A. M. Kuipers and M. V. S. Annaland, *Appl. Catal., A*, 2012, **433–434**, 96–108.
5 C. Karakaya, H. Zhu, C. Loebick, J. G. Weissman and R. J. Kee, *Catal. Today*, 2018, **312**, 10–22.
6 Z.-C. Jiang, C.-J. Yu, X.-P. Fang, S.-B. Li and H.-L. Wang, *J. Phys. Chem.*, 1993, **97**, 12870–12875.
7 D. Kiani, S. Sourav, J. Baltrusaitis and I. E. Wachs, *ACS Catal.*, 2019, **9**, 5912–5928.
8 Z. Aydin, A. Zanina, V. A. Kondratenko, J. Rabeah, J. Li, J. Chen, Y. Li, G. Jiang, H. Lund, S. Bartling, D. Linke and E. V. Kondratenko, *ACS Catal.*, 2022, **12**, 1298–1309.
9 H. O. Torshizi, A. N. Pour, A. Salimi and M. Ghadamyari, *Front. Chem. Sci. Eng.*, 2024, **18**, 1–11.
10 H. O. Torshizi, A. Nakhaei Pour, A. Salimi and Z. Nezhadalibaghan, *J. Chem. Technol. Biotechnol.*, 2024, **99**, 405–414.
11 S. Sourav, Y. Wang, D. Kiani, J. Baltrusaitis, R. R. Fushimi and I. E. Wachs, *Angew. Chem., Int. Ed.*, 2021, **60**, 21502–21511.
12 S. Sourav, D. Kiani, Y. Wang, J. Baltrusaitis, R. R. Fushimi and I. E. Wachs, *Catal. Today*, 2023, **416**, 113837.
13 D. Kiani, S. Sourav, W. Taifan, M. Calatayud, F. Tielens, I. E. Wachs and J. Baltrusaitis, *ACS Catal.*, 2020, **10**, 4580–4592.
14 C. A. Ortiz-Bravo, S. J. A. Figueroa, R. Portela, C. A. Chagas, M. A. Bañares and F. S. Toniolo, *J. Catal.*, 2022, **408**, 423–435.
15 K. Takanabe and E. Iglesia, *J. Phys. Chem. C*, 2009, **113**, 10131–10145.
16 Z. Aydin, V. A. Kondratenko, H. Lund, S. Bartling, C. R. Kreyenschulte, D. Linke and E. V. Kondratenko, *ACS Catal.*, 2020, **10**, 8751–8764.
17 Y. Wang, S. Sourav, J. P. Malizia, B. Thompson, B. Wang, M. R. Kunz, E. Nikolla and R. Fushimi, *ACS Catal.*, 2022, **12**, 11886–11898.
18 Q. Liu, R. Wang, R. Li, X. Wang, S. Zhao and C. Yu, *ACS Omega*, 2024, 36751–36760.
19 K. Takanabe and E. Iglesia, *Angew. Chem., Int. Ed.*, 2008, **47**, 7689–7693.
20 S. Yoshida, W. J. Movick, K. Obata, S. M. Sarathy and K. Takanabe, *Ind. Eng. Chem. Res.*, 2024, **63**, 11384–11391.
21 D. Li, S. Yoshida, B. Siritanaratkul, A. T. Garcia-Esparza, D. Sokaras, H. Ogasawara and K. Takanabe, *ACS Catal.*, 2021, **11**, 14237–14248.
22 K. Takanabe, A. M. Khan, Y. Tang, L. Nguyen, A. Ziani, B. W. Jacobs, A. M. Elbaz, S. M. Sarathy and F. (Feng) Tao, *Angew. Chem., Int. Ed.*, 2017, **129**, 10539–10543.
23 Z. Wei, W. J. Movick, K. Obata, S. Yoshida, D. Asada, T. Ikeda, A. Nakayama and K. Takanabe, *J. Phys. Chem. C*, 2024, **128**, 12969–12977.
24 Y. Zheng, A. Vidal-Moya, J. C. Hernández-Garrido, M. Mon and A. Leyva-Pérez, *J. Am. Chem. Soc.*, 2023, **145**, 24736–24745.
25 P. Mingueza-Verdejo, S. Hervàs-Arnandis, J. Oliver-Meseguer and A. Leyva-Pérez, *ACS Org. Inorg. Au*, 2024, **4**, 640.
26 A. Zanina, V. A. Kondratenko, H. Lund, J. Li, J. Chen, Y. Li, G. Jiang and E. V. Kondratenko, *ACS Catal.*, 2022, **12**, 15361–15372.
27 A. Zanina, V. A. Kondratenko, H. Lund, J. Li, J. Chen, Y. Li, G. Jiang and E. V. Kondratenko, *J. Catal.*, 2023, **419**, 68–79.
28 A. Palermo, J. Pedro, H. Vazquez and R. M. Lambert, *Catal. Lett.*, 2000, **68**, 191–196.
29 J. Kiwi, K. Ravidranathan Thampi, N. Mouaddib, M. Grätzel and P. Albers, *Catal. Lett.*, 1993, **18**, 15–26.
30 A. Erdohelyi, R. Németh, A. Hancz and A. Oszkó, *Appl. Catal., A*, 2001, **211**, 109–121.
31 A. Szöke and F. Solymosi, *Appl. Catal., A*, 1996, **142**, 361–374.
32 M. Ghiasi, A. Malekzadeh, S. Hoseini, Y. Mortazavi, A. Khodadadi and A. Talebizadeh, *J. Nat. Gas Chem.*, 2011, **20**, 428–434.
33 Z. Aydin, A. Zanina, V. A. Kondratenko, R. Eckelt, S. Bartling, H. Lund, N. Rockstroh, C. R. Kreyenschulte, D. Linke and E. V. Kondratenko, *Catal. Sci. Technol.*, 2021, **11**, 5827–5838.
34 S. Hou, Y. Cao, W. Xiong, H. Liu and Y. Kou, *Ind. Eng. Chem. Res.*, 2006, **45**, 7077–7083.

